Synthesis, Structure, and Properties of $La_{1-x}Sr_xTiO_3$ ($0 \leq x \leq 1$)

Joseph E. Sunstrom IV,[†] Susan M. Kauzlarich,*[,†] and Peter Klavins[‡]

Departments of Chemistry and Physics, University of California, Davis, California 95616

Received September 4, 1991. Revised Manuscript Received November 25, 1991

The search for a new superconductor in an early transition metal oxide prompted the investigation of the $La_{1-x}Sr_xTiO_3$ series of compounds. The solid solution $La_{1-x}Sr_xTiO_3$ ($0 \leq x \leq 1$) has been prepared by arc melting stoichiometric amounts of $SrTiO_3$ and $LaTiO_3$. Single-phase samples can be made for the entire stoichiometry range. The polycrystalline samples have been characterized using microprobe, thermogravimetric analysis, powder X-ray and neutron diffraction, temperature-dependent magnetization, and dc resistivity. The compounds crystallize in the orthorhombic space groups *Pbnm* ($x \leq 0.30$) and *Ibmm* ($0.30 < x < 0.80$), and the cubic space group *Pm3m* ($x \geq 0.80$). The *Pbnm* structure exists in two forms, O′-orthorhombic ($x < 0.10$) and O-orthorhombic ($0.10 \leq x \leq 0.30$), which are a result of Jahn–Teller distortion. The samples $x = 0.00$, 0.05 are canted antiferromagnets which exhibit a net ferromagnetic moment below 150 K and temperature-independent magnetism from 150 to 300 K. All other compositions show temperature-independent magnetism from 160 to 300 K with some samples ($x \geq 0.50$) displaying paramagnetism in the low-temperature range. The temperature dependent resistivity measurements show that the samples are metallic ($x \leq 0.70$) and semiconducting ($x = 0.90$). The $x = 0.80$ sample undergoes a semiconductor–metal transition. The properties of these materials are discussed in reference to the phenomenological phase diagram for perovskites proposed by Goodenough and high-T_c superconductivity.

Introduction

Research on metal oxide ceramics in the past 5 years has been primarily focused on superconducting systems.[1] Since the discovery of high-T_c superconductivity in $A_xLa_{2-x}CuO_4$ (A = Ba, Sr) ($T_c \approx 40$ K),[2] there has been a renewed interest in the optimization of superconducting properties in existing compounds in addition to the development of new superconducting oxides. Copper oxides such as $A_xLa_{2-x}CuO_4$ and $YBa_2Cu_3O_{7-y}$ ($T_c \approx 90$ K)[3] are found to exhibit high-temperature superconductivity. The superconducting transition temperatures of these compounds are higher than predicted by the number of states at the Fermi level and thus are defined as "high-T_c" compounds.[1b] $BaBi_{1-x}Pb_xO_3$ ($T_c \approx 13$ K)[4] also exhibits this type of superconductivity and using the above definition is arguably the first high-T_c superconductor. Reexamination of bismuth oxides has also produced $Ba_{1-x}K_xBiO_3$ ($T_c \approx 30$ K),[5] which currently has the highest critical temperature for any ceramic not containing copper. Oxides based on copper and bismuth are the only high-T_c superconducting ceramic compounds discovered to date. In principle, it may be possible to prepare high-T_c compounds based on a d^1 metal. $LiTi_2O_4$ ($T_c \approx 11$ K)[6] and $SrTiO_{3-x}$ ($T_c \approx 0.5$ K)[7] are two examples of superconducting compounds with a d^1 titanium metal cation. There are examples of Na_xAO_3 (A = Mo, W, Re)[8] bronzes which are superconducting, and recently superconductivity has been reported for several niobium oxide compounds.[9] The goal of this study is to examine titanium oxide compounds which show potential as d^1 high-T_c superconductors.

A set of requirements for superconductivity, proposed by Matthiass in 1957[10] and updated by Sleight in 1988,[11] can be categorized by four major features: electronic structure, macroscopic electrical properties, covalency of metal oxygen linkage, and metastability.

Ceramic high-T_c superconductors all contain either a fraction of an electron or hole in the valence electronic shell. One way to achieve either an s^x or d^x (where x is nonintegral) is through mixed valency of the transition or main-group metal. Sleight has proposed a mechanism to explain Cooper pair formation based on mixed valency or disproportionation of oxidation states.[12-14] In this mechanism, two single electron states are combined to form the diamagnetic Cooper pair and an empty state. This disproportionation mechanism requires that the state containing the single electron be nondegenerate. In addition, this single electron state must be diluted, otherwise magnetic ordering may result.

The electrical properties of high-T_c compounds appear to be similar. The superconducting phases predominantly lie near a metal–insulator border. The undoped compounds such as $BaBiO_3$ and La_2CuO_4 tend to be poor normal-state conductors. For example, progressively doping $BaBiO_3$ (a semimetal) with $BaPbO_3$ (a semiconductor) eventually causes a metal-to-insulator transition which is where the superconducting state lies.[15]

[†] Department of Chemistry.
[‡] Department of Physics.

(1) For a review, see, for example: (a) *Physics Today* **1991**, *44*, 22. (b) Cava, R. J.; Batlogg, B.; Krajewski, J. J.; Peck, W. F., Jr.; Rupp, L. W., Jr. *J. Less-Common Met.* **1990**, *164-165*, 749. (c) Müller-Buschbaum, H. *Angew. Chem., Int. Ed. Engl.* **1989**, *28*, 1472.
(2) Bednorz, J. G.; Muller, K. A. *Z. Phys. B: Condensed Matter* **1986**, *64*, 189.
(3) Wu, M. K.; Ashburn, J. R.; Torng, C. J.; Hor, P. H.; Meng, R. L.; Gao, L.; Huang, Z. J.; Wong, Y. Q.; Chu, C. W. *Phys. Rev. Lett.* **1987**, *58*, 908.
(4) Sleight, A. W.; Gillson, J. L.; Bierstedt, P. E. *Solid State Commun.* **1975**, *17*, 27.
(5) (a) Cava, R. J.; Batlogg, B.; Krajewshi, J. J.; Farrow, R. C.; Rupp, L. W., Jr.; White, A. E.; Short, K. T.; Peck, W. F., Jr.; Kometani, T. V. *Nature* **1988**, *332*, 814. (b) Mattheis, L. F.; Gyorgy, E. M.; Johnson, D. W., Jr. *Phys. Rev. B* **1988**, *37*, 3745.
(6) (a) Harrison, M. R.; Edwards, P. P.; Goodenough, J. B. *Philos. Mag. B* **1985**, 52, 679. (b) McCallum, R. W.; Johnston, D. C.; Luengo, C. A.; Maple, M. B. *J. Low Temp. Phys.* **1976**, *25*, 177. (c) Johnston, D. C.; Prakash, H.; Zachariasen, W. H.; Viswanthan, R. *Mater. Res. Bull.* **1973**, *8*, 777.
(7) Schooley, J. J.; Hosler, W. R.; Cohen, M. L. *Phys. Rev. Lett.* **1964**, *12*, 474.
(8) (a) A_xWO_3: Sweedler, A. R.; Raub, C.; Matthias, B. T. *Phys. Lett.* **1965**, *15*, 108. (b) A_xMoO_3, A_xReO_3: Sleight, A. W.; Butler, T. A.; Bierstedt, P. E. *Solid State Commun.* **1969**, *7*, 299.
(9) Geselbracht, M. J.; Richardson, T. J.; Stacy, A. M. *Nature* **1990**, *345*, 324.
(10) Matthias, B. T. *Prog. Low Temp. Phys.* **1957**, *2*, 138.
(11) Sleight, A. W. *Mater. Res. Soc. Symp. Proc.* **1988**, *99*, 3.
(12) Sleight, A. W. *High Temperature Superconducting Materials*; Hatfield, W. E., Miller, J. H., Eds.; Dekker: New York, 1988; p 1-36.
(13) Sleight, A. W. NIST Special Publication 804; *Proceedings of the International Conference of the Chemistry of Electronic Ceramic Materials*; Davies, P. K., Roth, R. S., Eds.; 1991; p 325.
(14) Sleight, A. W. *Science* **1988**, *242*, 1519.

0897-4756/92/2804-0346$03.00/0

Oxide superconductors have no close metal–metal contacts, which means that conduction is through metal–oxygen–metal linkages. These linkages must be covalent enough to support metallic conductivity. High covalency may also aid in stabilizing unusual oxidation states of the metal. Covalency of the metal–oxygen bonds can be increased by placing highly electropositive cations such as Ba^{2+} and Sr^{2+} around the M–O octahedra or planes.

Metastability may also be an important factor in high-T_c superconductivity.[16] There are a number of instabilities associated with ceramic superconductors which are best illustrated by example with $YBa_2Cu_3O_{7-x}$. The most obvious example is the orthorhombic-to-tetragonal transition which is a structural instability. In addition, an oxygen stoichiometry of seven is thermodynamically unstable in this compound.[17] There is also an electrical instability (normal-to-superconducting) in the compound.[18]

There are several structure types in the ternary titanium oxide system that may be manipulated synthetically in order to meet all the requirements mentioned above. $LaTiO_3$ crystallizes in the $GdFeO_3$ structure type (*Pbnm*) which is an orthorhombically distorted ABO_3 perovskite.[19,20] The d_{xy} orbital on Ti is nondegenerate, satisfying the requirement for a single electron state. The system $La_{1-x}Sr_xTiO_3$ ($0 < x < 1$) is a mixed-valent titanium oxide which has a d^{1-x} electronic configuration or a fraction of an electron in the d shell. The single electron states can be sufficiently diluted through control of the titanium valence by controlling the La/Sr ratio. $LaTiO_3$ has an electrical resistivity of approximately 10^{-2} Ω cm,[21] which can be classified as a poor metal while $SrTiO_3$ is an insulator. It is expected that at some composition in the solid-solution series of $LaTiO_3$ and $SrTiO_3$ a metal–insulator transition and perhaps a superconducting state will occur. Although covalency of the Ti–O bond is hard to quantify, in $LaTiO_3$ it is sufficient enough to support metallic conductivity. Introduction of a basic cation such as Sr^{2+} will increase the covalency of the Ti–O bond. In addition, as x increases in the system $La_{1-x}Sr_xTiO_3$, there will be a transition from the orthorhombic to the cubic structure, leading to a structural instability. Finally, the solid-solution formation of $LaTiO_3$ with $SrTiO_3$ will destroy the magnetic ordering ($LaTiO_3$ is a canted antiferromagnet with an ordering temperature of 125 K)[22] which in turn may force an electronic instability leading to superconductivity. This paper focuses on the synthesis and properties of the solid solutions of $LaTiO_3$[19-25] with $SrTiO_3$.[26]

Experimental Section

Materials. TiO_2 (99.999%) and $SrCO_3$ (99.999%) were purchased from Johnson Matthey. They were dried for 24 h at 120 °C prior to use. Ti_2O_3 (99+%) was used as purchased from Alfa Chemical. The oxygen content of Ti_2O_3 was characterized by thermogravimetric analysis and was determined to have the formula $Ti_2O_{2.158(8)}$. La_2O_3 (99.999%, Research Chemical) was heat treated at 1300 °C for 24 h prior to use.

Synthesis. $SrTiO_3$ was synthesized from TiO_2 and $SrCO_3$ by standard ceramic techniques.

Stoichiometric amounts of La_2O_3, $Ti_2O_{2.158(8)}$, and TiO_2 were arc melted under argon to form the black solid $LaTiO_3$. The oxygen content of the $LaTiO_3$ was determined by thermogravimetric analysis. All $LaTiO_3$ samples used for synthesis of the solid solution series, $La_{1-x}Sr_xTiO_3$, had an O:Ti ratio of 3.00 ± 0.02.

Solid solutions of $La_{1-x}Sr_xTiO_3$ ($0 \le x \le 1$) were prepared by arc melting stoichiometric amounts of $LaTiO_3$ and $SrTiO_3$ under an argon atmosphere.

Structure. X-ray powder diffraction data were obtained using an Enraf-Nonius Guinier camera equipped with a Johansson monochromator (Cu $K\alpha_1$ radiation). Finely ground samples were placed on a piece of cellophane tape with 5–10% silicon added as an internal standard. By fitting to a quadratic function, the five observed silicon diffraction lines were correlated to their known diffraction angles. Calculated powder patterns for $LaTiO_3$ (*Pbnm*) and $SrTiO_3$ (*Pm3m*) were made using the computer program POWDER.[27] A least-squares fitting program was used to calculate lattice parameters for the series (Table I). The lattice parameters of $SrTiO_3$ and $LaTiO_3$ are in agreement with their respective literature values.

A second set of X-ray diffraction data was obtained on a Siemens D-500 powder diffractometer with Cu $K\alpha$ radiation. The powder data, shown in Figure 1, were examined to check peak splitting, peak shapes, and intensity values. Powder X-ray diffraction data were obtained at room temperature for all samples. In addition, a low-temperature X-ray scan was made at 10 K for the $x = 0.40$ sample using a closed-cycle refrigerator attached to the goniometer.

Table I. Lattice Parameters (Å) Obtained from Guinier X-ray Powder Diffraction for $La_{1-x}Sr_xTiO_3$

x	a, Å	b, Å	c, Å	vol, Å^3
0.00	5.629 (2)	5.612 (1)	7.915 (1)	250.02 (12)
0.05	5.601 (3)	5.595 (1)	7.912 (1)	247.91 (12)
0.10	5.592 (5)	5.581 (2)	7.900 (2)	246.56 (23)
0.20	5.586 (4)	5.568 (3)	7.885 (3)	245.04 (24)
0.30	5.577 (5)	5.555 (3)	7.861 (3)	243.52 (24)
0.40	5.575 (1)	5.555 (1)	7.842 (1)	242.72 (7)
0.50	5.573 (1)	5.542 (1)	7.827 (2)	241.74 (8)
0.60	5.561 (1)	5.536 (1)	7.824 (2)	240.86 (8)
0.70	5.552 (1)	5.529 (2)	7.814 (2)	239.74 (9)
0.80	3.9079 (6)			59.68 (3)
0.90	3.9064 (6)			59.61 (4)
1.00	3.9056 (6)			59.57 (3)

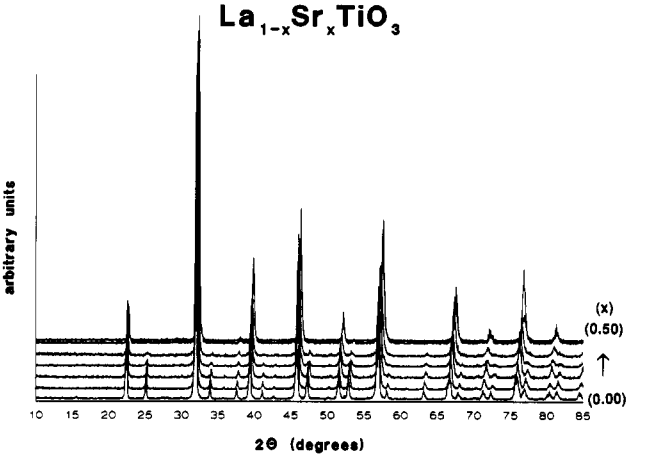

Figure 1. Powder diffractometer data of $La_{1-x}Sr_xTiO_3$ for (from bottom) x = 0.00, 0.05, 0.10, 0.20, 0.30, 0.40, 0.50.

(15) Sleight, A. W. *Chemistry of High Temperature Superconductors*; Nelson, D. L., Whittingham, M. S., George, T. F., Eds.; American Chemical Society: Washington DC, 1987; p 2–12.
(16) Sleight, A. W. *Phys. Today* **1991**, *June*, 24.
(17) Garzon, F. H.; Raistrick, I. D. NIST Special Publication 804; *Proceedings of the International Conference of the Chemistry of Electronic Ceramic Materials*; Davies, P. K., Roth, R. S., Eds.; 1991; p 373.
(18) Poole, C. P., Jr.; Datta, T.; Farach, H. A. *Copper Oxide Superconductors*; John Wiley and Sons: New York, 1988.
(19) MacLean, D. A.; Ng, H.-N.; Greedan, J. E. *J. Solid State Chem.* **1979**, *30*, 35.
(20) Eitel, M.; Greedan, J. E. *J. Less-Common Met.* **1986**, *116*, 95.
(21) MacLean, D. A.; Greedan, J. E. *Inorg. Chem.* **1981**, *20*, 1025.
(22) Greedan, J. E. *The Rare Earths in Modern Science and Technology*; McCarthy, G. J., Silber, H. E., Rhyne, J. J., Eds.; Plenum: New York, 1982; Vol. 3.
(23) Bazuev, G. V.; Shievkin, G. P. *Izv. Akad. Nauk SSR. Neorg. Mater.* **1978**, *14*, 267.
(24) Goral, J. P.; Greedan, J. E. *J. Magn. Magn. Mater.* **1983**, *37*, 315.
(25) Greedan, J. E. *J. Less-Common. Met.* **1985**, *111*, 335.
(26) Megaw, H. D. *Proc. Phys. Soc. (London)* **1946**, *A189*, 261.
(27) Clark, C. M.; Smith, D. K.; Johnson, G. A. A FORTRAN II program for calculating X-ray diffraction patterns, Version 5; Department of Geosciences, Pennsylvania State University, University Park, PA, 1973.

Table II. Selected Bond Distances (Å) and Angles (deg) for $La_{1-x}Sr_xTiO_3$ Obtained from Rietveld Analysis of Neutron Powder Diffraction Data

composition (x)	0.05	0.30	0.50
	Distances, Å		
Ti–O1	2.020 (1)	1.995 (1)	1.984 (1)
Ti–O2a	2.027 (1)	1.950 (1)	1.972 (1)
Ti–O2b	2.038 (1)	2.037 (1)	1.972 (1)
	Angles, deg		
Ti–O1–Ti	156.24 (1)	159.20 (1)	161.91 (1)
Ti–O2–Ti	154.32 (1)	163.39 (1)	170.47 (1)

Table III. Refinement Summaries from Neutron Powder Diffraction[a]

	$La_{0.95}Sr_{0.05}TiO_3$	$La_{0.7}Sr_{0.03}TiO_3$	$La_{0.5}Sr_{0.5}TiO_3$
space group	*Pbnm*	*Pbnm*	*Ibmm*
d_{min}, Å	0.500	0.500	0.500
N_{obs}	3606	3603	3610
N_{var}	27	27	27
N_{ref}	1261	1259	652
R_{pw}	0.0517	0.0712	0.0618
R_p	0.0348	0.0552	0.0472
χ^2	2.188	3.018	2.952
A	−0.108 (5)	−0.109 (4)	−0.375 (6)
E, μm^2	2 (1)	7 (2)	5 (2)
$(\Delta/\sigma)_{max}$	0.01	0.03	0.01

[a] A and E are absorption and extinction coefficients, respectively.

Room-temperature neutron diffraction data were obtained for three samples (x = 0.05, 0.30, 0.50) using the high-intensity powder diffractometer at the LANSCE facility, Los Alamos. Rietveld profile fitting[28] was completed using the computer program GSAS.[29] Atom positions and isotropic thermal parameters were refined to convergence for the +153° detector bank. Corrections were applied for both extinction and absorption due to large particle sizes in the sample. The initial atomic positions for the samples, x = 0.05, 0.30 were taken from $LaTiO_3$.[20] The data refined satisfactorily in the *Pbnm* space group for the x = 0.05 (R_p = 3.48%, R_{pw} = 5.17%, $R_{pw(expected)}$ = 3.49%) and x = 0.30 (R_p = 5.52%, R_{pw} = 7.12%, $R_{pw(expected)}$ = 4.10%) samples varying 28 parameters for each sample in the final refinement. The data for the 0.50 sample did not refine in the *Pbnm* space group but could be refined in the *Ibmm* space group (R_p = 4.72%, R_{pw} = 6.18%, $R_{pw(expected)}$ = 3.59%) varying 24 parameters in the final refinement. The initial atomic positions for the x = 0.50 sample were taken from $Pr_{1-x}Ba_xMnO_3$.[30] The atomic fractions were not refined, due to correlations with the thermal parameters. Selected bond distances and angles are given in Table II. Tables of structure refinement and positional and thermal parameters are given in Tables III and IV (six background parameters, scale factor, zero and four profile coefficients were refined for all samples).[29] Figures of observed, calculated, and difference profiles are available as supplementary materials.

Elemental Analysis. Elemental analysis of La, Sr, and Ti were completed on a Cameca SX-50 microprobe. $SrTiO_3$ and $LaTiO_3$ were used as standards. Samples were mounted in a plastic holder using epoxy, polished with Al_2O_3 powder, and carbon coated prior to analysis. The experimental results are given in Table V.

Oxygen stoichiometry was determined using a Du Pont Instrument Model 951 thermogravimetric analyzer. The microbalance on the thermogravimetric unit was calibrated before each experiment. Approximately 100 mg of sample was placed in a platinum boat hanging from the microbalance. The samples were heated from 25 to 1000 °C at 5 °C/min in 50 cm^3/min flowing O_2. The oxidation products of the samples, determined by powder X-ray diffraction, were $La_2Ti_2O_7$ and $SrTiO_3$. Some reduction experiments were completed using the same experimental conditions as above with 50 cm^3/min of 6% H_2 in N_2 substituted for oxygen. The oxygen stoichiometries are given in Table V.

Table IV. Refined Positional and Thermal Parameters from Neutron Powder Diffraction

atom	x	y	z	U_{iso}[a]
	$La_{0.95}Sr_{0.05}TiO_3$ (*Pbnm*)			
La(1)/Sr(1)[b]	0.9992 (2)	0.0366 (2)	0.25	89 (3)
Ti(1)	0.00	0.50	0.00	27 (4)
O(1)	0.0731 (6)	0.4884 (4)	0.25	67 (5)
O(2)	0.7110 (4)	0.2907 (4)	0.0409 (2)	60 (4)
	$La_{0.7}Sr_{0.3}TiO_3$ (*Pbnm*)			
La(1)/Sr(1)[b]	0.9878 (3)	0.0252 (4)	0.25	37 (5)
Ti(1)	0.00	0.50	0.00	18 (6)
O(1)	0.0631 (8)	0.4967 (9)	0.25	3.16 (6)
O(2)	0.7200 (8)	0.2759 (8)	0.0244 (4)	118 (6)
	$La_{0.5}Sr_{0.5}TiO_3$ (*Ibmm*)			
La(1)/Sr(1)[b]	0.9985 (8)	0.00	0.25	168 (3)
Ti(1)	0.00	0.50	0.00	136 (4)
O(1)	0.0560 (5)	0.50	0.25	76 (4)
O(2)	0.75	0.25	0.0209 (3)	197 (5)

[a] Thermal motion correction $T = \exp[-8\pi^2 U_{iso} \sin^2\theta/\lambda^2]$, U_{iso} shown as $\times 10^4$ Å^2. [b] Cation site occupanices constrained to their stoichiometric values, and the site is full.

Table V. Cation and Oxygen Stoichiometries for $La_{1-x}Sr_xTiO_3$ Obtained from Microprobe and Thermogravimetric Analysis, Respectively[a]

$La_{1.07(6)}TiO_{2.98}$	$La_{0.53(2)}Sr_{0.53(3)}TiO_{3.01}$
$La_{0.97(6)}Sr_{0.11(4)}TiO_{3.00}$	$La_{0.4}Sr_{0.6}TiO_{2.98}$
$La_{0.85(3)}Sr_{0.23(4)}TiO_{3.01}$	$La_{0.3}Sr_{0.7}TiO_{2.97}$
$La_{0.74(4)}Sr_{0.31(3)}TiO_{3.02}$	$La_{0.2}Sr_{0.8}TiO_{2.97}$
$La_{0.6}Sr_{0.4}TiO_{2.99}$	$La_{0.1}Sr_{0.9}TiO_{2.97}$

[a] Cation stoichiometries without standard deviations are as prepared and not determined from microprobe data.

Magnetic and Electronic Characterization. A Quantum Design SQUID magnetometer was used to make magnetic measurements. The samples with composition $0 \le x \le 0.1$ were cooled in a field of 1 T to 5 K. The magnetization vs temperature data were taken in an applied field of 10 G (5–170 K) and 1 T (170–300 K). For x = 0.1, 0.2, the applied field was 1000 G from 5 to 170 K and 1 T from 170 to 300 K. At compositions of $x > 0.2$, 1 T was applied from 5 to 300 K. Hysteresis loops for samples of composition $0 < x < 0.1$ were completed at 10 K with an applied field range of −5 to 5 T. All samples were screened for the Meissner effect at 5 K and for compositions, $0.1 < x \le 0.5$, down to 2 K.

Dc resistivity measurements were made using the standard four-probe technique. The samples were cut into regular shapes on the order of 1.5 × 1.5 × 1.5 mm^3. Platinum wire (0.002 in.) leads were attached using silver epoxy. A Keithley Model 224 current source (1 mA) and a Keithley Model 181 nanovoltmeter were used to measure the resistivity of the samples within the 10–300 K temperature range.[31] Thermal voltages were minimized by reversal of the current bias.

Results and Discussion

Synthesis and Composition. The synthetic method (arc melting) used to prepare the solid solution, $La_{1-x}Sr_xTiO_3$, was chosen in order to control the titanium valency in the solid solution. In studies of the dielectric properties of doped $SrTiO_3$, La^{3+} is doped into $SrTiO_3$ by the solid-state reaction of La_2O_3, SrO, and TiO_2.[32,33] The

(28) (a) Rietveld, H. M. *Acta Crystallogr.* **1967**, *22*, 151. (b) Rietveld, H. M. *J. Appl. Crystallogr.* **1969**, *2*, 65.
(29) Larson, A. C.; Von Dreele, R. B. GSAS—Generalized Crystal Structure Analysis System, Los Alamos National Laboratory Report No. LA-UR-86-748, 1987.
(30) Jirak, Z.; Pollert, E.; Andersen, A. F.; Grenier, J.-C.; Hagenmüller, P. *Eur. J. Solid State Inorg. Chem.* **1990**, *27*, 421.
(31) Sunstrom, J. E., IV; DCRES, a QuickBASIC program for resistivity data collection and statistical analysis, University of California, Davis; 1990, unpublished.
(32) Tien, T. Y.; Hummel, F. A. *Trans. Brit. Ceram. Soc.* **1969**, *66*, 233.
(33) Bouwma, J.; De Vries, K. J.; Burggraaf, A. *J. Phys. Status Solidi A* **1976**, *35*, 281.

results of this direct reaction of the oxides in air produces $Sr_{1-x}La_{2/3x}TiO_3$ which is a Ti(IV) compound.[32] In the ABO_3 perovskite, $Sr_{1-x}La_{2/3x}TiO_3$, two La^{3+} ions are distributed over three Sr^{2+} sites in order to maintain electroneutrality in the sample. Reaction of the metal oxides to make the La-rich side of the $SrTiO_3$–$LaTiO_3$ solid solution is not a viable method (even in high vacuum) due to excess oxygen in the reaction stoichiometry. Direct reaction of $SrTiO_3$ with $LaTiO_3$ offers two advantages: (1) the enthalpy of mixing of the compounds is low due to their similar structures and (2) there is no excess oxygen that could cause the vacancy mechanism described above. In this reaction, a Ti(III) perovskite is diluted by a Ti(IV) perovskite to form $La_{1-x}Sr_xTiO_{3\pm y}$, an ABO_3 compound. By changing x, optimum control of the Ti^{3+}/Ti^{4+} ratio can be attained.

Thermal gravimetric analysis of $LaTiO_3$ and $La_{1-x}Sr_xTiO_3$ samples are consistent with the oxygen stoichiometry nearly 3.00 for all samples (cf. Table V). For $SrTiO_3$, it has been shown that the oxygen content can be as low as 2.5.[7] Recently, single crystals of the oxygen-deficient compound $SrTiO_{2.72}$ have been prepared and characterized.[34] Considering the fact that $SrTiO_3$ can be prepared oxygen deficient and the extreme synthetic conditions used to prepare the series, $La_{1-x}Sr_xTiO_3$, it is somewhat surprising that the oxygen content is stoichiometric for these compounds. It may be harder to create oxygen defects around the higher charge of the La(III) cation, since the oxygen is in the coordination sphere of the La(III)/Sr(II) cation. Attempts to reduce the oxygen stoichiometry by reduction under 6% H_2/94% N_2 up to 1000 °C were unsuccessful. $LaTiO_3$ and $La_{1-x}Sr_xTiO_3$ are slightly oxygen and water sensitive and degrade slowly over time if left in air.

Microprobe analysis on selected samples provided a verification of the stoichiometries of the cations and the homogeneity of the samples. The experimental results given in Table V are consistent with the theoretical stoichiometries. The compositions in Table V are based on an average of data taken on 20 random spots on the sample. The low standard deviations quoted indicate homogeneous samples.

X-ray powder diffraction data indicates that single-phase materials can be made for the entire series. The lattice parameters for the series obtained by Guinier X-ray powder diffraction are given in Table I. Parts a and b of Figure 2 show plots of cell volume and lattice parameter versus composition ($0 \le x \le 0.70$), respectively. The compounds are orthorhombic ($GdFeO_3$ structure) for $x \le 0.30$ and reflections were indexed in the space group *Pbnm*. This structure allows smaller (La,Sr)–O distances by buckling the Ti–O octahedra. The $GdFeO_3$ structure type is a result of ionic sizes and occurs in ABO_3 perovskites when the Goldschmidt tolerance factor, t, is less than 0.9.[35] The Goldschmidt tolerance factor is given below where R_A and R_B and R_O are the radii for the cations (A and B) and the oxygen anion, O^{2-}:

$$t = (R_A + R_O)/\sqrt{2}(R_B + R_O) < 0.9$$

The Goldschmidt tolerance factors for all compositions of $La_{1-x}Sr_xTiO_3$ were calculated using the equation above, R_A and R_B were calculated from the weighted average for the composition (La^{3+}, 1.30 Å; Sr^{2+}, 1.40 Å; Ti^{3+}, 0.81 Å; Ti^{4+}, 0.745 Å) and R_O = 1.21 Å.[36] The tolerance factors for

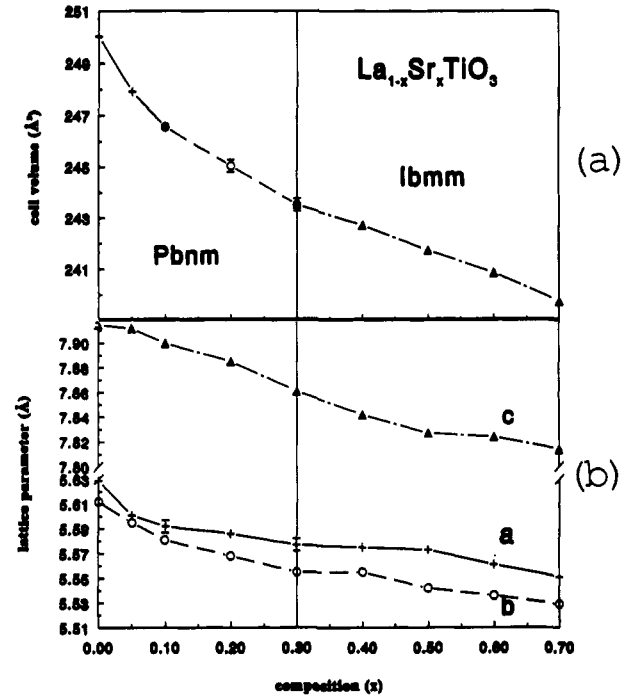

Figure 2. (a) Plot of cell volume vs composition and (b) plot of lattice parameters vs composition of $La_{1-x}Sr_xTiO_3$ for $0.00 \le x \le 0.70$.

$La_{1-x}Sr_xTiO_3$ indicate that the $GdFeO_3$ structure (*Pbnm*) is stable for $x \le 0.30$ which is consistent with the experimental data. The structure change can clearly be seen in the diffractometer traces shown in Figure 1. The bottom trace is $LaTiO_3$ and the top two are the x = 0.40, 0.50 samples. The smaller peaks which are characteristic of the *Pbnm* structure disappear with increasing Sr content indicating a transition to a higher symmetry structure.

The plot of cell volume vs composition (Figure 2a) for the solid solution series shows a change in slope at x = 0.10. The change in the cell volume can be understood in terms of the observed changes in the a and b cell parameters. The plot of the orthorhombic lattice parameters a, b, and c in Figure 2b shows a clear dependence on x, although not in accordance with Vegard's rule. The difference between a and b decreases until x = 0.10 and then increases ($0.10 > x > 0.30$) while the c parameter decreases linearly with composition. To better understand these structural changes, neutron powder diffraction data were obtained for two of the orthorhombic compositions. The space group, *Pbnm*, was verified for the x = 0.05, 0.30 compositions by Rietveld refinement of the neutron data. There are two slightly inequivalent Ti–O–Ti angles in these compounds indicated by Ti–O1–Ti and Ti–O2–Ti (Table II). One is oriented along the c axis and the other is in the ab plane. This tilts the Ti–O octahedra in two ways: along the [001] axis and within the (001) plane as shown in Figure 3a. In the $LaTiO_3$ structure, there are two crystallographically different oxygens, O1 and O2, and three different Ti–O bonds. The Ti–O1 bond, 2.028 (1) Å, is oriented along c, Ti–O2a and Ti–O2b with bond lengths of 2.044 (1) and 2.032 (1) Å, respectively, are oriented along the ab plane.[20] The Ti–O1 distance decreases with increasing Sr content from 2.028 Å in $LaTiO_3$[20] to 2.020 Å for x = 0.05, 1.995 Å for x = 0.30 to 1.984 Å for x = 0.50, consistent with the linear decrease of the c parameter. The two Ti–O2 distances are almost equivalent at x = 0.05 (2.027 (1) and 2.038 (1) Å) and significantly different at x = 0.30 (1.950 (1) and 2.037 (1) Å). It appears that as the concentration of Sr increases, the longer Ti–O2a

(34) Gong, W.; Yun, H.; Ning, Y. B., Greedan, J. E.; Datars, W. R.; Stager, C. V. *J. Solid State Chem.* **1991**, *90*, 320.
(35) Goodenough, J. B. *Prog. Solid State Chem.* **1975**, *5*, 145.
(36) Shannon, R. D.; Prewitt, C. T. *Acta Crystallogra.* **1969**, *B25*, 925.

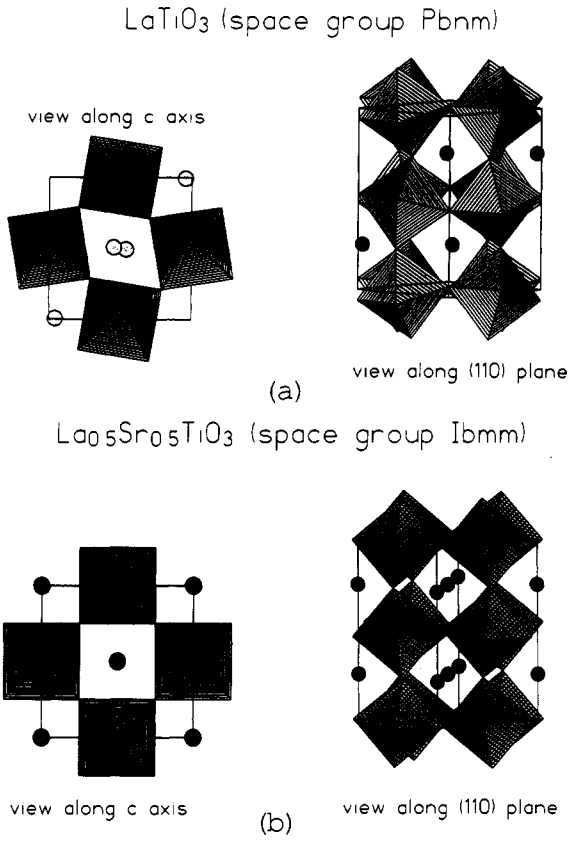

Figure 3. Titanium is in the center of the octahedra. (a) *Pbnm* structure determined from refined neutron data for the $x = 0.05$ $La_{1-x}Sr_xTiO_3$ sample. The left view, down the *c* axis, shows buckling in the *ab* plane. The right view, down the [110] plane, shows buckling along the *c* axis. (b) *Ibmm* structure determined from refined neutron data for the $x = 0.50$ $La_{1-x}Sr_xTiO_3$ sample. Right view, down the [110] plane, still shows buckling along the *x* axis. However, the left view, down the *c* axis, does not show any buckling in the *ab* plane.

bond length approaches the shorter Ti–O2b bond length until the Sr composition reaches about $x = 0.10$. When $x > 0.10$, the Ti–O2b bond distance is always longer than the Ti–O2a bond distance until $x > 0.30$. The deviation at $x = 0.10$ in the plot of volume versus composition is attributed to this cross over in bond lengths for Ti–O2a and Ti–O2b.

There are two substructures for the $GdFeO_3$ (*Pbnm*) structure type, denoted O′-orthorhombic and O-orthorhombic, in compounds which exhibit Jahn–Teller distortion. The O′-orthorhombic structure consists of a cooperative Jahn–Teller distortion superimposed over the O-orthorhombic structure.[37] This octahedral rearrangement that is observed as *x* increases is consistent with a structural change from the O′-orthorhombic to the O-orthorhombic *Pbnm* structure. For a d^1 octahedral system, the Jahn–Teller theorem requires the octahedra to distort such that the lone electron is in a nondegenerate t_{2g} state. Although the Jahn–Teller theorem does not predict how a compound will distort, a d^1 octahedral system should compress along the *z* axis allowing the lone electron to occupy the lower energy d_{xy} orbital. On the other hand, an elongation along the *z* axis would cause the lone electron to occupy one of the lower energy doubly degenerate d_{xz}, d_{yz} orbitals. If the electron occupies the d_{xz}, d_{yz} orbitals, the Jahn–Teller theorem requires further distortion to break the degeneracy of these two orbitals. The lattice parameters of the O-orthorhombic structures (a_0, b_0, c_0) are related to the cubic perovskite (*Pm3m*) lattice parameter, a_c, as follows: $a_0 \approx b_0 \approx \sqrt{2}a_c$ and $c_0 \approx 2a_c$. The O-orthorhombic structure has a lattice parameter ratio $c_0/a_0 \geq \sqrt{2}$. The O′-orthorhombic structure is characterized by the lattice parameter ratio $c_0/a_0 < \sqrt{2}$ which indicates a compression along the $c(z)$ axis. $LaTiO_3$ and $La_{0.95}Sr_{0.05}TiO_3$ have c_0/a_0 ratios less than $\sqrt{2}$, indicating Jahn–Teller distortion.[35]

The structure could best be indexed according to the space group *Ibmm* for the compositions $0.30 < x < 0.80$. This is verified by the Rietveld refinement of the neutron data on the $x = 0.50$ sample. Although the diffraction patterns appear to be cubic, the peaks are broad, indicating some small distortion (cf. Figure 1). X-ray powder diffraction data taken at 10 K for the $x = 0.40$ sample did not show any resolved splitting for the broad peaks. The space group *Ibmm* is an orthorhombic space group whose symmetry components are intermediate between the orthorhombic space group, *Pbnm* ($LaTiO_3$) and the highly symmetric, cubic space group *Pm3m* ($SrTiO_3$).[38] Perovskite structures crystallizing in the *Ibmm* space group are characterized by two widely different M–O–M angles, whereas in the *Pbnm* space group, these angles are nearly the same. The Ti–O2–Ti angle determined for the $x = 0.50$ composition is 170.47 (1)°, much closer to 180° in the *ab* plane than the Ti–O1–Ti angle, 161.91 (1)°, that is along the *c* axis. The octahedra in the *Ibmm* space group are tilted only along the [001] direction (cf. Figure 3b).

For $x \geq 0.80$, the samples are indexed as cubic (*Pm3m*). In the *Pm3m* space group, all Ti–O–Ti angles are 180° and the octahedra are not tilted and the Ti–O distances is half of the cubic lattice parameter. The value for $x = 0.9$, $a = 3.9064$ (6) Å, is smaller than that reported for single crystals of the same stoichiometry (3.910 Å).[39] Metal stoichiometries were not verified for $x = 0.9$ in this work or in ref 39, and there is probably some stoichiometric deviation in both samples. The lattice parameters are smaller than predicted based on the size of the cations and anions,[36] indicating that the Ti(III) content is lower than expected in both samples. The cubic lattice parameter decreases from $x = 0.80$ to $x = 1.00$ due to the increasing amount of Ti(IV) and the decreasing Ti–O bond distance.

Magnetic and Electronic Properties. Goodenough has devised a phenomenological phase diagram for perovskites which predicts the macroscopic electrical and magnetic properties as a function of *b*, the transfer integral.[35] Since there are no close metal–metal contacts in perovskites, the properties are determined by the interaction between metal ions through an intervening oxygen anion. The magnitude of the transfer integral, while hard to quantify, is related to the degree of overlap between the metal and oxygen orbitals. In Ti(III) perovskites, *b* is proportional to the degree of overlap between the titanium t_{2g} and oxygen $2p_\pi$ orbitals. There are several values of *b*, where there are transitions from one group of magnetic and electrical properties to another. One such value in the collective electron regime, denoted b_m, delineates the semiconducting, magnetically ordered phase from the metallic, Pauli paramagnetic phase. For $b < b_m$, the material is semiconducting and magnetically ordered. Metallic conductivity and Pauli paramagnetism are observed for $b > b_m$. It has been suggested that the transfer integral for $LaTiO_3$ changes with temperature and is close to b_m.[24] Upon addition of Sr into $LaTiO_3$, the Ti–O–Ti angle ap-

(37) Goodenough, J. B.; Longo, J. M. In *Landolt-Börnstein Tabellen*; New Series III/4a; Springer-Verlag: West Berlin, 1970.

(38) Bärnighausen, H. *Acta Crystallogr., Ser. A* **1975**, *S3*, 31.

(39) Higuchi, M.; Aizawa, K.; Yamaya, K.; Kodaira, K. *J. Solid State Chem.* **1991**, *92*, 573.

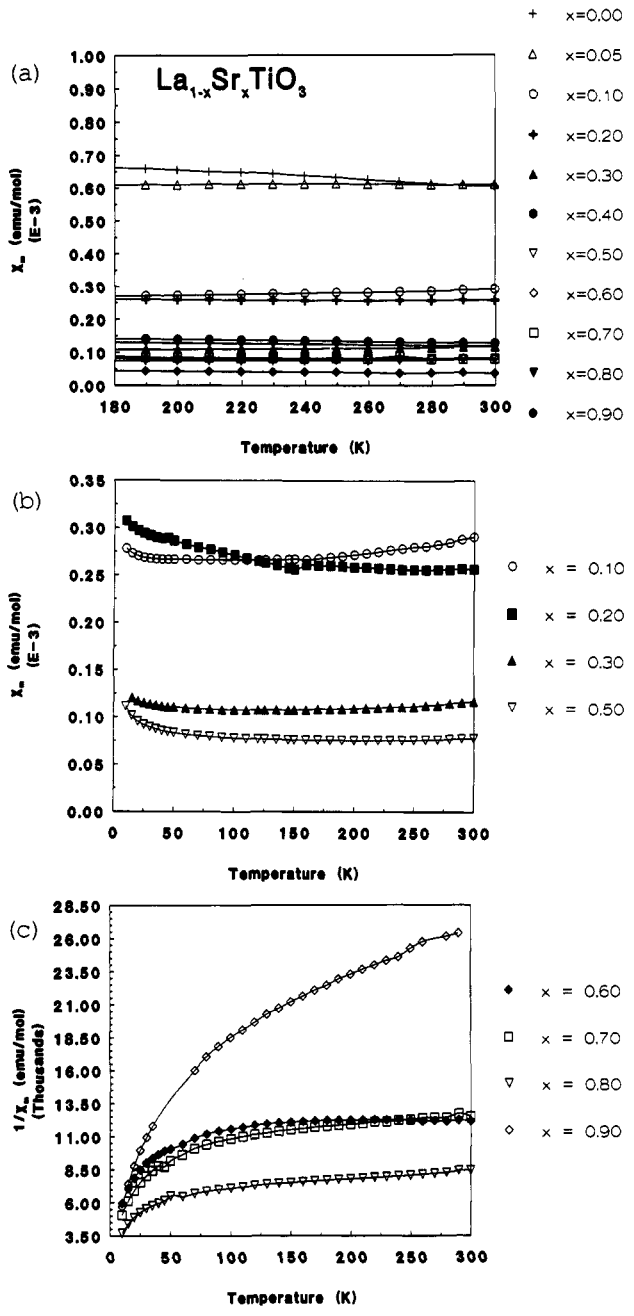

Figure 4. (a) Molar magnetic susceptibilities versus temperature (180–300 K) for $La_{1-x}Sr_xTiO_3$ for (from top) x = 0.00, 0.05, 0.10, 0.20, 0.30 0.50, 0.60, 0.70, 0.80, 0.90. (b) Molar magnetic susceptibilities versus temperature (5–300 K) for $La_{1-x}Sr_xTiO_3$ for (from top) x = 0.10, 0.20, 0.30, 0.50. (c) Inverse molar magnetic susceptibilities versus temperature (5–300 K) of $La_{1-x}Sr_xTiO_3$ for (from top) x = 0.90, 0.70, 0.60, 0.80.

proaches 180° which increases the transfer integral, b, by providing a better π orbital overlap between the titanium and oxygen. Because the transfer integral for $LaTiO_3$ is near b_m, one would predict that with increasing Sr content metallic behavior and Pauli paramagnetism will dominate until the electrons in the t_{2g} orbital of titanium are depleted.

Figure 4a shows temperature-dependent magnetic susceptibility from 180 to 300 K for the entire range of samples. The data are temperature independent in this region. $LaTiO_3$ is a canted antiferromagnet (canting angle 1°) which exhibits parasitic ferromagnetism[24] and the saturation moment obtained from the hysterisis loop (μ_{sat} = 10.9×10^{-3} μ_B/molecule) is in good agreement with that obtained by Greedan et al. Introduction of Ti^{4+} into the

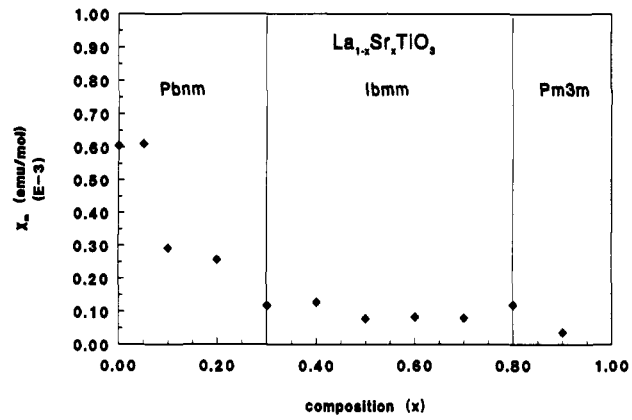

Figure 5. Molar magnetic susceptibilities (T = 300 K) vs composition, x, of $La_{1-x}Sr_xTiO_3$.

titanium sublattice disrupts the magnetic ordering. The saturation moment decreases as x increases, with a value of 3.7×10^{-3} μ_B/molecule obtained for x = 0.05. This magnetic order is destroyed in the $La_{1-x}Sr_xTiO_3$ solid solution when x = 0.1.[40] The susceptibilities for the samples ($0.1 \leq x \leq 0.50$) are temperature independent in the 10–300 K temperature range with the x = 0.5 sample showing some paramagnetism in the low-temperature (10–50 K) range (cf. Figure 4b). The remaining samples ($x \geq 0.60$) are temperature independent (150–300 K) with a paramagnetic contribution at low temperature (cf. Figure 4c). The high-temperature data for the x = 0.90 sample is clearly temperature dependent, indicating localized electrons and nonmetallic behavior. None of the samples showed a Meissner effect at 5 K and for $x \leq 0.5$ samples, no Meissner effect was observed down to 2 K.

One of the terms in the temperature-independent susceptibility, the Pauli susceptibility, is proportional to the density of states (DOS) at the Fermi level. The temperature independent susceptibility value of 635 (20) $\times 10^{-6}$ emu/mol for the $LaTiO_3$ is slightly smaller than that previously reported for single-crystal measurements.[24] This value is indicative of a high DOS at the Fermi level. The temperature-independent susceptibilities range from 635 (20) $\times 10^{-6}$ emu/mol for $LaTiO_3$ to 47 (1) $\times 10^{-6}$ emu/mol for the $La_{0.1}Sr_{0.9}TiO_3$ sample and are plotted as a function of composition in Figure 5. This indicates that the DOS is decreasing with increasing Sr content which is consistent with removing electrons from a partially filled band. However, the temperature-independent susceptibilities do not change smoothly with increasing x, suggesting that a rigid band model is not valid for this solid-solution series. This is consistent with the changes in structure observed in the solid-solution series. The largest changes in temperature-independent susceptibility occur in the stoichiometry range that maintains the *Pbnm* structure as indicated in Figure 5. In this range, the structure is changing due to the distortion of the Ti–O octahedra which also perturbs the crystal field around Ti. A change in band structure can be attributed to these crystal field effects. The d_{xy} orbital is half filled (x = 0.00) and nondegenerate in the *Pbnm* structure; as the structure changes from *Pbnm* to *Ibmm* to *Pm3m*, the d_{xy}, d_{xz}, and d_{yz} orbitals become degenerate (t_{2g}) and there is a significant drop in the magnitude of the temperature-dependent susceptibilities. These changes are consistent with a narrow band (d_{xy}) in

(40) Kauzlarich, S. M.; Sunstrom, J. E., IV; Klavins, P. NIST Special Publication 804; *Proceedings of the International Conference of the Chemistry of Electronic Ceramic Materials*; Davies, P. K., Roth, R. S., Eds.; 1991; p 217.

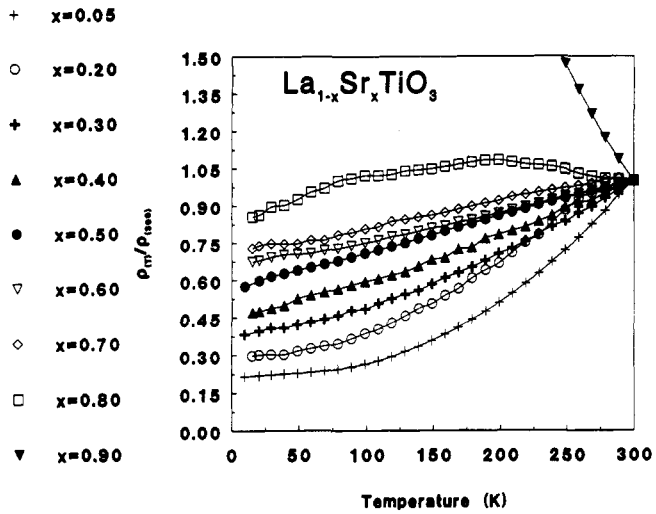

Figure 6. Normalized resistivities vs temperature of $La_{1-x}Sr_xTiO_3$ for (from bottom) x = 0.05, 0.20, 0.30, 0.40, 0.50, 0.60, 0.70, 0.80, 0.90.

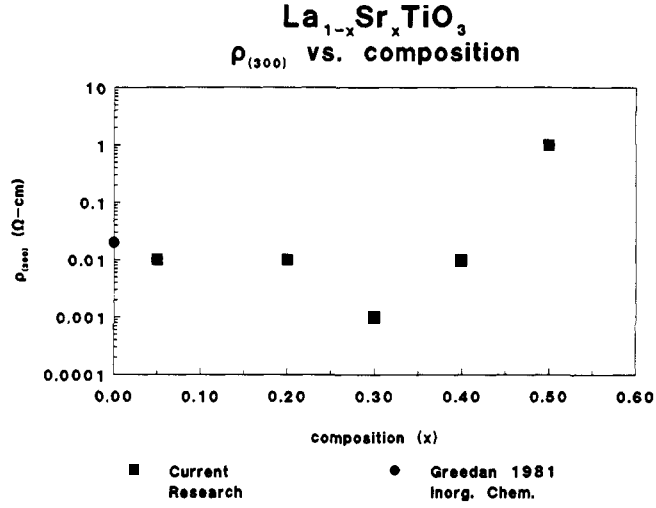

Figure 7. Room-temperature resistivities vs composition of $La_{1-x}Sr_xTiO_3$ for $0 \le x \le 0.50$.

the case of the *Pbnm* structure and a wider band (t_{2g}) in the *Ibmm* and *Pm3m* structures.

The normalized resistivity vs temperature curves for the solid solution are shown in Figure 6 for compositions $0.05 \le x \le 0.90$. The samples show a metallic temperature dependence when $x \le 0.70$. The resistivity data have an exponential temperature dependence for $x \le 0.30$, indicating that the resistivity is due predominantly to phonon scattering. For $x \ge 0.40$, the temperature dependence of the resistivity data is linear and still metallic. The $x = 0.80$ sample goes through a semiconductor–metal transition at approximately 190 K, and the $x = 0.90$ sample exhibits semiconducting behavior. This result for the $x = 0.90$ sample differs from the recent resistivity studies on single crystals of $Sr_{1-x}La_xTiO_3$ ($x \le 0.1$) which show these materials to be metallic.[39] The source of the discrepancy between these data and the single-crystal data is attributed to differences in Ti(III) concentration in the samples. The transition from metallic to insulating properties is most likely a result of the low carrier concentrations since the Ti–O–Ti angle of 180° allows optimal orbital overlap for conductivity. A plot of ln σ vs $1/T$ for the $x = 0.90$ sample yields a bandgap of 0.08 eV.

Figure 7 shows the room-temperature resistivity values as a function of composition, $0 \le x \le 0.50$. The resistivity decreases until $x = 0.30$ and then increases steadily. The resistivity should decrease with increasing Sr content due to a larger transfer integral, b. The sudden increase in resistivity after $x = 0.30$ is coincident with the structure change from the *Pbnm* structure to the *Ibmm* structure. The two Ti–O–Ti angles in the *Pbnm* phase are approximately the same which means the current pathway should be isotropic in the unit cell. In the *Ibmm* phase the Ti–O–Ti angle in the *ab* plane is much closer to 180° which provides a more favorable current path perpendicular to the *c* axis in the unit cell. For polycrystalline samples, in which the unit cells are oriented in random directions, this anisotropy may lead to the higher resistivity values. In addition, there is an unknown contribution to resistance from grain boundaries which will also lead to higher resistivity values compared to single-crystal data.

Summary

Single-phase samples can be prepared for the entire solid-solution series $La_{1-x}Sr_xTiO_3$. The electrical and magnetic properties in these samples are as predicted by the Goodenough phase diagram.[35] None of the samples exhibited superconducting properties over the temperature range measured. It is still possible that there is a superconducting state at very low temperatures, but these measurements were not pursued. There are some fundamental differences between the Ti–O and Cu–O systems which may account for the lack of high-temperature superconductivity. The conduction band of the Cu–O and Bi–O compounds is of σ^* symmetry, while Ti–O compounds have a π^* conduction band. The σ^* interaction affords better overlap between the metal–oxygen linkage in perovskite (corner shared octahedral) compounds. There may be a better chance for superconductivity in face- or edge-shared Ti–O compounds (e.g., $LiTi_2O_4$)[6] where overlap is increased for the π^* interaction. Another barrier to superconductivity for the Ti–O system may be the carrier type. Conductivity in the Ti–O system is achieved with electrons as the carriers (n-type), while for the Cu–O and Bi–O systems the conduction is through hole movement (p-type). Finally, although metallic conduction is possible through the Ti–O bond covalency, it may not be covalent enough to stabilize superconductivity. It has been suggested that Cu predominates in superconducting transition metal systems because there is no activation barrier to disproportionation of oxidation states which perhaps is mediated by the crystal structure.[41] Certainly, an activation barrier would be related to the covalency of the metal–oxygen bond. We are presently studying the effect of different cations around the Ti–O linkages in an attempt to increase their covalency as well as synthesizing other Ti–O structure types.

Acknowledgment. We thank Professor R. N. Shelton for use of the magnetometer, X-ray diffractometer, and TGA, Dr. T. Y. Kuromoto for help in obtaining microprobe and neutron data, and Professor D. J. Webb for useful discussion. The work has benefitted from the use of facilities at Manuel Lujan, Jr. Neutron Scattering Center, a national user facility funded as such by the DOE/Office of Basic Energy Sciences. The work was supported by National Science Foundation Solid State Chemistry Grant DMR-8913831.

Registry No. $La_{1-x}Sr_xTiO_3$ (x = 0.00), 12201-04-6; $La_{1-x}Sr_xTiO_3$ (x = 0.05), 137486-43-2; $La_{1-x}Sr_xTiO_3$ (x = 0.10), 137486-38-5; $La_{1-x}Sr_xTiO_3$ (x = 0.20), 114966-27-7; $La_{1-x}Sr_xTiO_3$ (x = 0.30), 138855-74-0; $La_{1-x}Sr_xTiO_3$ (x = 0.40), 137486-10-3; $La_{1-x}Sr_xTiO_3$

(41) Hagenmuller, P.; Pouchard, M.; Grenier, J. C. *Solid State Ionics* 1990, *43*, 7.

(x = 0.50), 138855-75-1; $La_{1-x}Sr_xTiO_3$ (x = 0.60), 120501-49-7; $La_{1-x}Sr_xTiO_3$ (x = 0.70), 120501-50-0; $La_{1-x}Sr_xTiO_3$ (x = 0.80), 120501-51-1; $La_{1-x}Sr_xTiO_3$ (x = 0.90), 120501-52-2; $La_{1-x}Sr_xTiO_3$ (x = 1.00), 12060-59-2; $La_{1-x}Sr_xTiO_3$ (x = 0.00–1.00), 138855-76-2.

Supplementary Material Available: Figures of observed, calculated, and difference profiles obtained from the neutron powder diffraction data (4 pages). Ordering information is given on any current masthead page.

Straight-Chain Carbamyl Compounds for Second Harmonic Generation

Cecil V. Francis* and George V. D. Tiers

3M Corporate Research Laboratory, Box 33221, St. Paul, Minnesota 55133-3221

Received September 9, 1991. Revised Manuscript Received November 20, 1991

Straight-chain alkyl and analogous polymethylene esters and amides of nitrophenyl carbamic acids (urethanes and ureas) have been found to yield acentric crystals having nonlinear optical properties. These crystals displayed powder second harmonic generation efficiencies ranging from 0 to 154 times that of urea, depending on the crystallizing solvent and the crystallizing conditions employed. Powder X-ray diffraction D spacings were employed to characterize the exact crystal form of each sample of material studied.

Introduction

The possibility of using organic compounds in nonlinear optical (NLO) devices has generated much interest recently because numerous types of molecules are available for investigation. Some substituted aromatic compounds are known to exhibit large optical nonlinearities, and these are enhanced if the molecule has both donor and acceptor groups bonded at opposite ends of the conjugated system.[1] The potential utility for very-high-frequency applications of organic materials having large second-order (and third-order) nonlinearities is greater than that for conventional inorganic electrooptic materials because of the higher dielectric constants of the latter. Furthermore, the properties of organic materials can often be varied to optimize mechanical and thermooxidative stability as well as laser damage threshold.

For a material to be useful in second harmonic generation (SHG), the active NLO moiety must exist in a macroscopically acentric environment. To fulfill this criterion, molecular structures intended for NLO applications frequently include a chiral moiety. It is true that this does not ensure that the NLO-active moiety will be properly oriented in the acentric environment to produce high SHG; nevertheless, as is clearly demonstrated by chiral carbamic acid derivatives,[2] this technique is a reliable one for making molecules which form acentric SHG-active crystals. It is also possible to introduce macroscopic acentricity in a material by the use of an electric field either for poling an amorphous material[3] or for biasing the molecules to crystallize in a desired acentric form.[4]

This report describes a series of acentric achiral compounds which may be regarded as providing a novel route for inducing acentricity in crystals. These straight-chain carbamyl compounds, some of which may also be considered for Langmuir–Blodgett film formation, are characterized by powder X-ray diffraction (XRD) D spacings in the exact crystal forms studied for SHG activity.

Experimental Section

The urethanes and ureas were all synthesized from 4-nitrophenyl isocyanate by similar methods; therefore, representative syntheses are shown. The 4-nitrophenyl isocyanate was purified by dissolving it in dry hot toluene followed by filtering to remove all undissolved solids. The principal impurity, bis(4-nitrophenyl)urea, mp 324 °C (dec), is extremely insoluble in most solvents. The filtrate can either be evaporatively cooled to effect crystallization of the 4-nitrophenyl isocyanate or be used as is. Most of the urethanes have been previously reported,[5] but we find slightly higher melting points in most cases. Melting points were obtained on a modified Buchi–Tottoli apparatus, metal-calibrated to the International Temperature Scale of 1990.[6] Differential scanning calorimetry was performed under nitrogen (Du Pont 2100 DSC apparatus; nonsealed sample containers) and verified, by absence of anomalous endotherms, that the SHG samples were not solvates, and the melting points generally agreed with the capillary determination within ±1 °C.

Infrared spectroscopy was used to verify the presence of urethane and urea groups, and proton NMR with integration was used to confirm the structure of each compound.

Synthesis of 1-(11-bromoundecyl)-4-nitrophenyl carbamate: Freshly purified 4-nitrophenyl isocyanate (Aldrich, 9.0 g, 0.055 mol) was dissolved in 100 mL of dry ether in a 250-mL round-bottom flask. To this were added 13.8 g (0.055 mol) of 11-bromo-1-undecanol (Aldrich) and 3 drops of dibutyltin dilaurate in 120 mL of ether. After the exotherm had subsided, the reaction was refluxed for about 2 h before the yellow precipitate was recovered by filtration. Recrystallization from ethanol gave extremely pale yellow crystals in excellent yield (>95%), mp 122–123 °C.

Synthesis of N-octadecyl-N'-4-nitrophenyl urea: n-Octadecylamine (Aldrich, 1.35 g, 0.005 mol) and freshly purified 4-nitrophenyl isocyanate (Eastman, 0.83 g, 0.005 mol) were dissolved in 25 mL of toluene in a 50-mL Erlenmeyer flask fitted with air condenser and heated for about 2 h on a steam bath. The yellowish precipitate which formed on cooling was filtered off and recrystallized from acetone to yield 1.59 g of whitish solid (76%), mp 121–122 °C.

(1) Levine, B. F.; Bethea, C. G.; Thurmond, C. D.; Lynch, R. T.; Bernstein, J. L. *Appl. Phys.* **1979**, *50*, 2523.
(2) Tiers, G. V. D. U.S. Patent 4,818,899, 1989.
(3) Khanarian, G., Ed. Nonlinear Optical Properties of Organic Materials II. *SPIE Proc.* **1989**, *1147*, 101.
(4) (a) Hampsch, H. L.; Yang, J.; Wong, G. K.; Torkelson, J. M. *Macromolecules* **1988**, *21*, 526. (b) Watanabe, T.; Yoshinaga, K.; Fichou, D.; Miyata, S. *J. Chem. Soc., Chem. Commun.* **1988**, 250.
(5) *Beilsteins Handbuch der Organischen Chemie*; Springer-Verlag: Berlin; E III, Vol. 12, part 3, 1972, pp 1607–9, and references therein.
(6) Tiers, G. V. D. *Anal. Chim. Acta* **1990**, *237*, 241.

0897-4756/92/2804-0353$03.00/0